Single Ho^{3+}-Doped Upconversion Nanoparticles for High-Performance T_2-Weighted Brain Tumor Diagnosis and MR/UCL/CT Multimodal Imaging

Dalong Ni, Wenbo Bu, Shengjian Zhang, Xiangpeng Zheng, Ming Li, Huaiyong Xing, Qingfeng Xiao, Yanyan Liu, Yanqing Hua, Liangping Zhou, Weijun Peng, Kuaile Zhao, and Jianlin Shi**

Multimodal bio-imaging has attracted great attention for early and accurate diagnosis of tumors, which, however, suffers from the intractable issues such as complicated multi-step syntheses for composite nanostructures and interferences among different modalities like fluorescence quenching by MRI contrast agents (e.g., magnetic iron oxide NPs). Herein, the first example of T_2-weighted MR imaging of Ho^{3+}-doped upconversion nanoparticles (UCNPs) is presented, which, very attractively, could also be simultaneously used for upconversion luminesence (UCL) and CT imaging, thus enabling high performance multi-modal MRI/UCL/CT imagings in single UCNPs. The new finding of T_2-MRI contrast enhancement by integrated sensitizer (Yb^{3+}) and activator (Ho^{3+}) in UCNPs favors accurate MR diagnosis of brain tumor and provides a new strategy for acquiring T_2-MRI/optical imaging without fluorescence quenching. Unlike other multi-phased composite nanostructures for multimodality imaging, this Ho^{3+}-doped UCNPs are featured with simplicity of synthesis and highly efficient multimodal MRI/UCL/CT imaging without fluorescence quenching, thus simplify nanostructure and probe preparation and enable win–win multimodality imaging.

1. Introduction

Magnetic resonance imaging (MRI) is becoming increasingly important in tumor diagnosis due to its high resolution of soft tissue and noninvasive approach.[1] However, the inherent drawbacks of low sensitivity and limited visualization for subtle changes in pathology have seriously hindered its further biological application.[1b] Fortunately, a large amount of exogenous contrast agents (CAs) have been explored to shorten longitudinal (T_1) or transverse (T_2) relaxation time of surrounding water protons in order to improve imaging quality and effectively acquire detailed lesion information.[2] Among them, superparamagnetic iron oxide nanoparticles (SPIONs) with various sizes and surface modifications have extensively served as T_2 contrast-enhancing agents for MRI owing to the high feasibility on detecting a lesion in T_2 weighted MR imaging,[1b,2b,3] However, SPIONs' inevitable magnetic susceptibility artifact is a great obstacle in clear imaging and distinguishing the lesions from background.[4] Moreover, the diagnosis efficiency is also significantly limited in single MR imaging mode, which can be overcome by other imaging modalities, such as fluorescence imaging with inherent ultra-high sensitivity.[5]

Actually, several methods have been developed to combine magnetic and fluorescent materials by using nanohybrids as MR and fluorescent bimodal imaging CAs. Typically, SPIONs have been widely combined with organic dyes or polymers,[6] and quantum dots (QDs).[7] Unfortunately, organic dyes suffer from poor photostability and significant autofluorescence, and meanwhile, QDs have been receiving great concerns for their harmful tissue photodamage and high potential Cd-cytotoxic risks. In contrast, upconversion nanoparticles (UCNPs), which can emit strong visible-to-NIR luminescence under the excitation of NIR light in the "optical transmission window" of biological tissues (750–1000 nm), have received great attentions due to their incomparable advantages such as enhanced tissue penetration depth, and much suppressed photo-damage and autofluorescence.[8] And these UCNPs combining with SPIONs for bimodal imaging can efficiently avoid the aforementioned drawbacks.[9] However, fluorescence quenching constitutes a common fatal flaw for all these fluorescent probes in practical applications as the black SPIONs have long been

Dr. D. Ni, Prof. W. Bu, Dr. H. Xing, Dr. Q. Xiao, Dr. Y. Liu, Prof. J. Shi
State Key Laboratory of High Performance Ceramics and Superfine Microstructure
Shanghai Institute of Ceramics
Chinese Academy of Sciences
Shanghai, 200050, P.R. China
E-mail: wbbu@mail.sic.ac.cn; jlshi@mail.sic.ac.cn
Dr. S. Zhang, Prof. L. Zhou, Prof. W. Peng, Prof. K. Zhao
Department of radiology
Shanghai Cancer Hospital
Fudan University
Shanghai, 200032, P.R. China
Prof. X. Zheng, Prof. M. Li, Prof. Y. Hua
Department of radiation oncology
Shanghai Huadong Hospital
Fudan University
Shanghai, 200040, P.R. China

DOI: 10.1002/adfm.201401609

considered as a traditional strong light absorber which could greatly weaken both the incident excitation light and fluorescence emission.[10] Taking QDs as an example, their quantum yield (QY) decreased remarkably from 11.4% to 1.1% after integrating with SPIONs.[7b] In addition, the preparation of these nanohybrids often involves complicated multi-step synthetic procedures, leading to high costs and less practical utility. As a result, how to explore a novel nanoprobe with excellent and win-win MR/fluorescence imaging performance instead of mechanical mixing of different function modalities is still a great challenge.

For MRI, most of the paramagnetic lanthanide ions such as Dy^{3+}, Ho^{3+}, Er^{3+}, Tm^{3+}, and Yb^{3+} exhibit relatively short electronic transverse relaxation time that mainly affects T_2 weighted MRI.[11] With the nature of paramagnetism, they will not distort the magnetic field on neighboring normal tissues and as a result, will generate no magnetic susceptibility artifact.[4a] Their proton relaxation is mainly induced via Curie mechanism, the contribution of which is proportional to the square of the effective magnetic moment of lanthanide ion.[12] Among them, Ho^{3+} (as well as Dy^{3+}) has the shortest electronic relaxation time and the highest effective magnetic moment (μ_{eff} = 10.6 μ_B) which will result in the most efficient T_2 relaxation among lanthanide ions.[13] More excitingly, Ho^{3+} is also frequently used as activator for upconversion luminescence imaging (UCL) when combined with sensitizer Yb^{3+} (μ_{eff} = 4.5 μ_B). Therefore, Ho^{3+}-doped UCNPs can offer an excellent combination between T_2-MR and fluorescence imaging without any aforementioned problems. In addition, the higher attenuation characteristics of Yb^{3+} and Ho^{3+} than Iodine (e.g., Yb: 3.88 $cm^2\ g^{-1}$; Ho: 3.49 $cm^2\ g^{-1}$ and I: 1.94 $cm^2\ g^{-1}$ at 100 KeV),[14] endow these NPs with higher contrast performance than clinical iobitridol for CT imaging, which gives additional high-resolution 3D anatomic structure details and is of significant medical complementation for MR and fluorescence imaging. However, surprisingly to the authors, reports on T_2-weighted MRI and MR/CT imaging of Ho^{3+}-doped UCNPs have not been found in literatures so far.

Our group has previously prepared a series of bioimaging nanoprobes, such as neck-formed SPIONs/UCNPs, and Au or TaO_x coated UCNPs for multimodal imaging.[15] However, besides the complicated synthetic procedures, the possible detachment of different imaging agents from heterogenous nanostructure remains an unsolved issue. In this study, we have successfully synthesized Ho^{3+}-doped $NaYbF_4$ with surface phospholipid-PEGylation (Lipo-UCNPs) for multimodal T_2-MRI/UCL/CT imaging in single NPs. In addition to intrinsic UCL and CT imaging due to the presence of heavy metal Yb/Ho in UCNPs, excellent T_2-MRI performance have been obtained by combined activators and sensitizers (e.g., Ho^{3+} and Yb^{3+}, respectively) within single UCNPs which effectively annihilated fluorescence quenching. More importantly, the remarkable T_2-MRI performance of Ho^{3+}-doped UCNPs has further been demonstrated by the efficient MR imaging of glioblastoma, which is the most lethal brain tumor and remains highly challenging for efficient detection because of its easy evasiveness to diagnosis.[16]

2. Results and Discussion

As schematically illustrated in **Figure 1**a, oleic acid (OA) coated $NaYbF_4$: Ho NPs (OA-UCNPs) were synthesized by a typical pyrolysis method.[17] These prepared NPs could be well dispersed in chloroform (Figure 1b and Supporting Information Figure S1a,b,S2a–d). The powder X-ray diffraction (XRD) patterns (Supporting Information Figure S1c,S2e) show that both

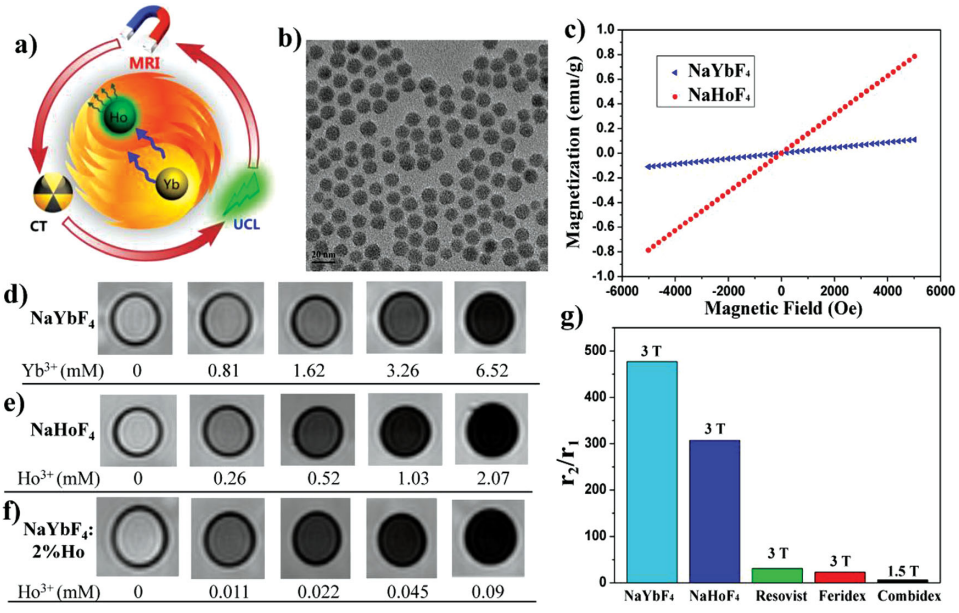

Figure 1. a) Schematic diagram of Ho^{3+}-doped UCNPs as the T_2-MRI/UCL/CT multimodal imaging. b) TEM images of $NaHoF_4$ in chloroform. c) *M–H* curves of $NaYbF_4$ and $NaHoF_4$ NPs at 300 K. T_2-weighted phantom MR images of d) Lipo-$NaYbF_4$, e) Lipo-$NaHoF_4$, and f) Lipo-UCNPs at different concentrations. g) Comparsion of r_2/r_1 values among the clinical negative CAs and the Ho^{3+}/Yb^{3+}-based NPs.

pure $NaYbF_4$ matrix and Ho^{3+}-doped $NaYbF_4$ NPs at varied Ho^{3+} concentrations have a cubic phase (Joint Committee on Powder Diffraction Standards-JCPDS, No. 27–1426), while $NaHoF_4$ NPs show hexagonal phase (JCPDS No. 49–1896). The energy dispersive X-ray (EDX) spectra confirm the existence of all expected elements (Na, Yb, Ho and F) in these nanoprobes (Figure S3, Supporting Information). The well known biomimetic DSPE-PEG_{2000}-NH_2 were then used to modify the hydrophobic NPs into hydrophilic environment through the van der Waals interactions between two hydrophobic tails of phospholipids and oleic acid ligands on NPs' surface.[18] Importantly, these amine-groups at ligand ends can be readily used for further surface modification by antibody or peptide conjugation. The as-prepared Lipo-UCNPs doped with 2% Ho^{3+} displays excellent water dispersity without any visible aggregation (Figure S4a,b, Supporting Information), which is further demonstrated by the hydrated size of 47.5 nm (Figure S4c, Supporting Information). Two new bands at ≈1646 and ≈1109 cm^{-1} in fourier transform infrared (FT-IR) spectrum (Figure S5, Supporting Information) of Lipo-UCNPs can be assigned to the amide groups and ether bond in PEG chains,[14b,19] indicating successful modification of DSPE-PEG_{2000}-NH_2. And due to positively charged amine groups on surface, Lipo-UCNPs shows a positive-zeta potential (15.5 ± 4.4 mV), contributing to the stable dispersion and high potential for further in vivo application.

The magnetization plots (M-H) reveal the paramagnetism of two kinds of NPs, with calculated magnetization values being 0.66 and 4.7 emu/g for $NaYbF_4$ and $NaHoF_4$ NPs, respectively, at 30 KOe (Figure 1c). Here, the much higher magnetization of $NaHoF_4$ NPs than that of $NaYbF_4$ NPs can be ascribed to the larger effective magnetic moment (μ_{eff}) of Ho^{3+} (μ_{eff} = 10.6 μ_B) than that of Yb^{3+} (μ_{eff} = 4.5 μ_B), which directly leads to remarkable difference of transverse relaxivity between $NaHoF_4$ (36.01 mM^{-1} s^{-1}) and $NaYbF_4$ (4.25 mM^{-1} s^{-1}) NPs (Figure S6, Supporting Information). T_2-weighted phantom MR images were obtained at 3.0 T for both $NaYbF_4$ and $NaHoF_4$ NPs and showed concentration-dependent signal enhancement (Figure 1d,e). It is demonstrated here that, both sensitizer Yb^{3+} and activator Ho^{3+} show excellent T_2-MRI contrast performance, indicating the important T_2-MRI contrast role of Ln ions in UCNPs. Recently, Gd-UCNPs as T_1-MRI CAs have been well documented since they were first reported by Prasad's group,[20] and great efforts have been made to optimize their MRI performance.[21] To benefit the fluorescent emission of UCNPs, much higher amount (15%–20%) of sensitizer Yb^{3+} than that of Gd^{3+} (≈2 mol%) was doped in Gd-UCNPs. As a result, the reported r_2 values of Gd-UCNPs, which were normalized to Gd^{3+} concentration, were much higher than their actual value due to the neglected specific relaxometric contribution of Yb^{3+}. For example, r_2 of Gd-UCNPs[15b] (e.g., Gd: <2.1 mol%; Yb: 20 mol%) was reported to be as high as 147.3 mM^{-1} s^{-1} with r_2/r_1 ratio of 12.9, as compared to r_2 value of 5.8 $mM^{-1}s^{-1}$ of Gd-DTPA with r_2/r_1 of 1.6.[22] Obviously, the r_2 and r_2/r_1 values of Gd-UCNPs was highly over-valued and did not fundamentally represent the real MRI performance. Herein, we demonstrate the T_2-MR contrast enhancement by integrating sensitizer and activator in single UCNPs.

By doping 2% Ho^{3+} into $NaYbF_4$, high performance T_2-MRI was obtained. The magnetization was extrapolated to be 0.78 emu/g at 30 KOe (Figure S7a, Supporting Information). T_2-relaxation time of water proton is shortened significantly from 190 ms to 30 ms (Figure S7b, Supporting Information) by Ho^{3+} doping and the corresponding T_2-weighted images become darker at increased Ln concentration (**Figure 2**f). It has been reported that the contrast in MRI depends on its r_1 and r_2 relaxivity as well as r_2/r_1 ratio, the higher the ratio of r_2/r_1, the better the efficiency of T_2 CA and vice versa for a T_1 CA.[23] It is noteworthy to mention that the obtained $NaYbF_4$ and $NaHoF_4$ NPs possess extremely high r_2/r_1 ratio of 477 and 307, respectively, at 3.0 T, which are much higher than that of clinically used negative CAs such as Combidex, Feridex, and Resovist (r_2/r_1 = 6, 22.6, and 31, respectively).[24] Moreover, Ln-based NPs (Ln≠Gd) have been demonstrated to be the potential ultrahigh

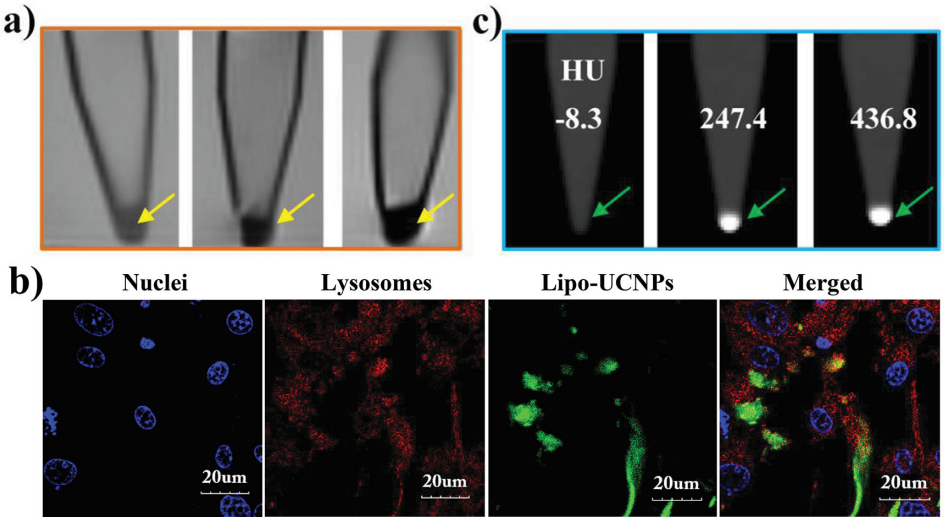

Figure 2. a) T_2-weighted MRI of U87MG cells incubated with Lipo-UCNPs at various concentrations (0, 400, and 800 μg mL^{-1}, respectively). b) Representative intracellular fluorescence distribution in U87MG cells after incubated with Lipo-UCNPs (800 μg mL^{-1}) for 2 h. c) CT images of U87MG cells incubated without Lipo-UCNPs (left), with different concentrations of Lipo-UCNPs (400, and 800 μg mL^{-1} for the middle and right).

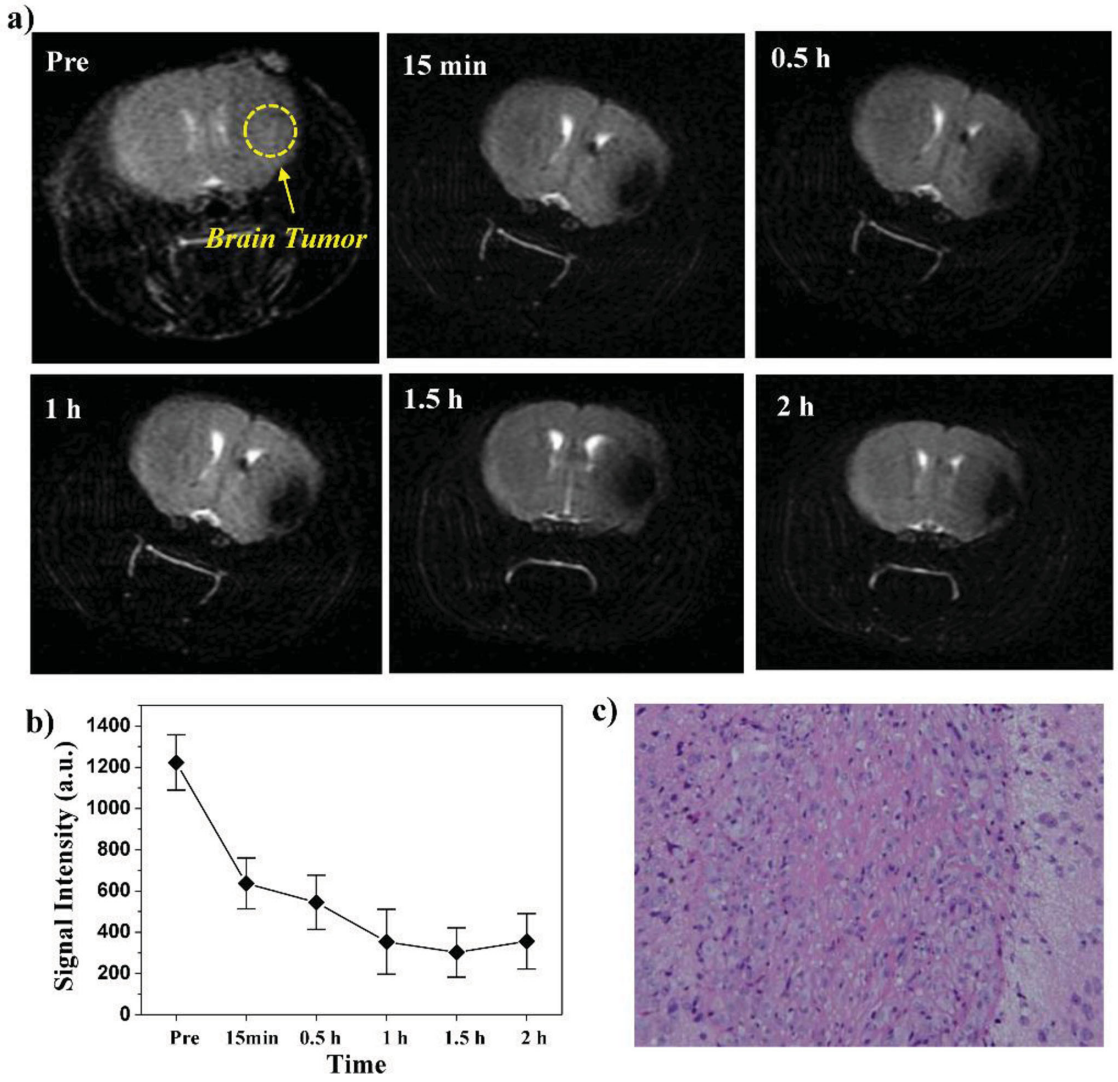

Figure 3. a) In vivo T_2-MR imaging of glioblastoma-bearing mice before and at various time points after intravenous injection of Lipo-UCNPs (30 mg Yb/Kg). b) Quantitative analysis result of signal intensity (SI) in the T_2-weighted MR images of brain tumor. c) H&E-staining of the tumor tissue from glioblastoma-bearing mice brain.

field T_2-weighted MR CAs,[11b,23b] because r_2 values of Ln-based NPs are approximately proportional to MR field strength as well as square of magnetization (M). Therefore, this negative contrast enhancement will become even stronger at higher MR field as the M increases strongly with increase of MR field strength.[25] Meanwhile, the above clinical negative CAs saturate their magnetization at around 1.5 T, disabling the enhancement in MRI contrast in further strength-enhanced ultrahigh MR field.[26] Therefore, the extremely high r_2/r_1 ratio of Ho^{3+}/Yb^{3+}-based NPs and magnetic field-dependent MRI contrast enhancement clearly reveal their high potential as excellent T_2 CA under elevated magnetic field because magnetization of materials continue to increase at magnetic field strength of >3.0 T.[13a]

The T_2-MRI contrast enhancement performance of Ho^{3+}-doped UCNPs was evaluated both in living cells and in vivo. We first studied in vitro cytotoxicity against human glioblastoma cells U87MG and normal brain capillary endothelial cells (BCECs) by a typical MTT assay (Figure S8, Supporting Information). It is shown that cell viability remains above 85% even after the co-incubation with an extremely high concentration (800 μg/mL) of Lipo-UCNPs for 12 h or 24 h, thereby demonstrating their remarkably low cytotoxicity. T_2-MR images further confirm that Lipo-UCNPs can be internalized by U87MG cells, and this internalization is concentration-dependent (Figure 2a). To demonstrate high-performance T_2-MRI of Ho^{3+}-doped UCNPs in vivo, we performed MR brain tumor imaging before and after intravenous injection of Lipo-UCNPs. As shown in **Figure 3**a, high contrast of brain tumor can be clearly observed as indicated by the arrow. This visible contrast maintained for over 2 h, which could be quantitatively measured by T_2-weight MR signal intensity (SI). The regions of interest (ROI) were localized in each MR image with fixed size and matching position. As shown in Figure 3b, the average SI value of brain tumor is remarkably reduced after injection, and even decreases to a maximal ≈75.3% in ≈1.5 h post-injection owing

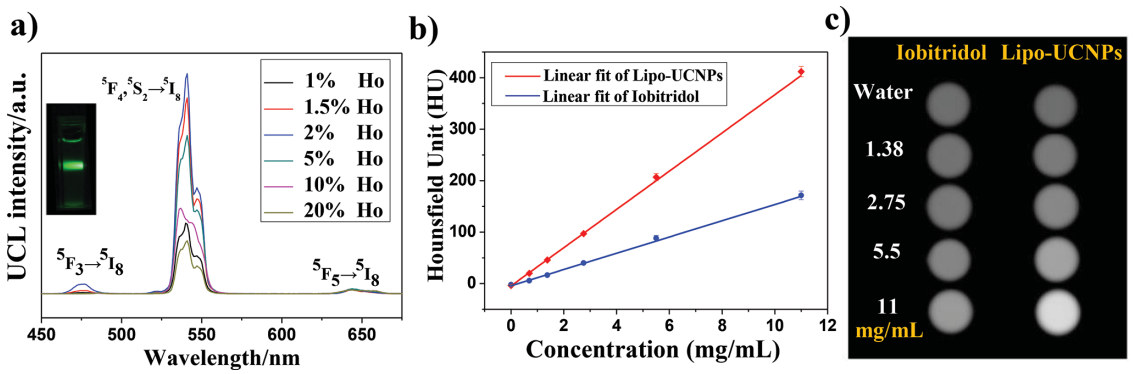

Figure 4. a) Room temperature UCL spectra of UCNPs at different Ho^{3+} doped concentrations. The spectra in (a) are normalized to Ho^{3+} 647 nm emissions. Insert shows the photograph of 2% Ho^{3+}-doped UCNPs under 980 nm excitation. b) HU measurements and c) CT images of Lipo-UCNPs and iobitridol at different concentrations.

to the efficient tumor accumulation by the enhanced permeability and retention (EPR) effect.[27] The hematoxylin and eosin (H&E)-stained tumor section from brain shows the presence of brain tumor (Figure 3c). Together, the above in vivo imaging experiments demonstrate the feasibility of Ho^{3+}-doped UCNPs as T_2-MRI CAs and their high-performance MR contrast for efficient brain tumor imaging without magnetic susceptibility artifact.

Furthermore, Yb^{3+} as a sensitizer has a larger absorption cross-section in the NIR region, which make $NaYbF_4$ a well-know host material for NIR-Vis UCL imaging.[14,28] Here, Ho^{3+}-doped $NaYbF_4$ exhibits a strong green light (540 nm, $^5F_4$, $^5S_2 \rightarrow {}^5I_8$) emissions under 980 nm excitation. And the corresponding emission intensity increases at the increased Ho^{3+} concentration where more Ho^{3+} become available to receive energy transfer from Yb^{3+}, which reaches the maximum at 2% Ho^{3+} (**Figure 4**a). Then emission intensity is considerably decreased when Ho^{3+} concentration increases from 5% to 20%, where the increased concentration of Ho^{3+} in host lattice will decrease Yb···Ho inter-atomic distance and thus facilitate back-energy-transfer from Ho^{3+} to Yb^{3+}, resulting in the decreased light emissions.[29] After modification with phospholipid-PEG-NH_2, no obvious change is observed in UCL spectrum (Figure S9, Supporting Information). By using confocal laser-scanning microscopy, green fluorescence is observed in U87MG cells after incubation with Lipo-UCNPs (Figure 2b). In addition, the Lyso Tracker for staining lysosome suggests that a number of Lipo-UCNPs have entered lysosomes while the rests residue in the cytoplasm. No fluorescent signals of Lipo-UCNPs are found in the nucleus, indicating that NPs could not cross the nuclear membrane.

Encouraged by the excellent performance of Lipo-UCNPs in vitro, in vivo T_2-MR as well as UCL imaging were carried out on Kunming mouse by intravenous administration of Lipo-UCNPs. As illustrated in **Figure 5**a, high contrast of liver is observed in both T_2-weighted coronal and transversal cross-section images and this high contrast remains for over 2 h. Moreover, the emission can be tuned to NIR region (800 nm), which is observed clearly in liver after intravenous administration of Lipo-UCNPs (2%Ho/2%Tm) for 2 h (Figure 5b,c), demonstrating the potential value of Lipo-UCNPs as fluorescence imaging probes for in vivo imaging. Herein, 2% Ho-doped Lipo-UCNPs can provide excellent T_2-MR contrast enhancement and enhanced UCL imaging. Using the Ho^{3+}/Yb^{3+} combination in fluorescent UCNPs for T_2-MRI can not only simplify material preparation for multimodal imaging, but also efficiently prevent the common problem of fluorescence quenching, which widely exists in combination between SPIONs and fluorescent materials.

Due to the high X-ray absorption coefficiency of Yb^{3+} and Ho^{3+} (e.g., Yb: 3.88 cm^2g^{-1}; Ho: 3.49 cm^2g^{-1} at 100 KeV), Ho^{3+}-doped UCNPs can also be used for CT imaging (Figure S10). Figure 4b-c present phantom CT images and HU values of Lipo-UCNPs and iobitridol of different concentrations, both of which exhibit remarkable signal enhancements at increased concentrations. The line slope of the HU value *vs* ion concentration for Lipo-UCNPs is about 37.2 HU L/g, much higher than that of iobitridol (15.8 HU L/g). Prior to using Lipo-UCNPs for in vivo CT imaging, cellular CT images in living cells confirm the efficient uptakes of Lipo-UCNPs of different concentrations and HU values are greatly increased from –8.3 to 436.8 (Figure 2c). In vivo CT imaging was further conducted by intravenously injecting Lipo-UCNPs to track the distribution of NPs at timed intervals (Figure 5d). An immediate enhancement of the signal of heart can be observed after injection and this contrast lasts for ≈30 min. Then the cardiac CT signal decreases while the enhancement of signal in liver and spleen continues for over 2 h (Figure 5d,e and Supporting Information Figure S12), which indicates that Lipo-UCNPs have a long in vivo blood circulation half-life ($t_{1/2}$ = 1.49 h, Figure S13, Supporting Information). This long-lasting circulation enables CAs to maintain a relative high concentration in blood stream which will benefit the uptake by the liver tumor for efficient imaging.[30] Then, the clinical iobitridol was used as comparison. As shown in Figure S11 (Supporting Information), iobitridol mainly accumulates in the urinary organs (kidney and bladder), and no contrast is observed in heart, liver and spleen, indicating the rapid vascular permeation and short circulation time of iobitridol in body (Figure S11,12, Supporting Information). These in vitro and in vivo CT imaging studies demonstrate the much better performance of CT imaging of Lipo-UCNPs than that of clinical iobitridol.

To investigate the harmful effect of Lipo-UCNPs, the short and long-term toxicity was assessed by histological changes in

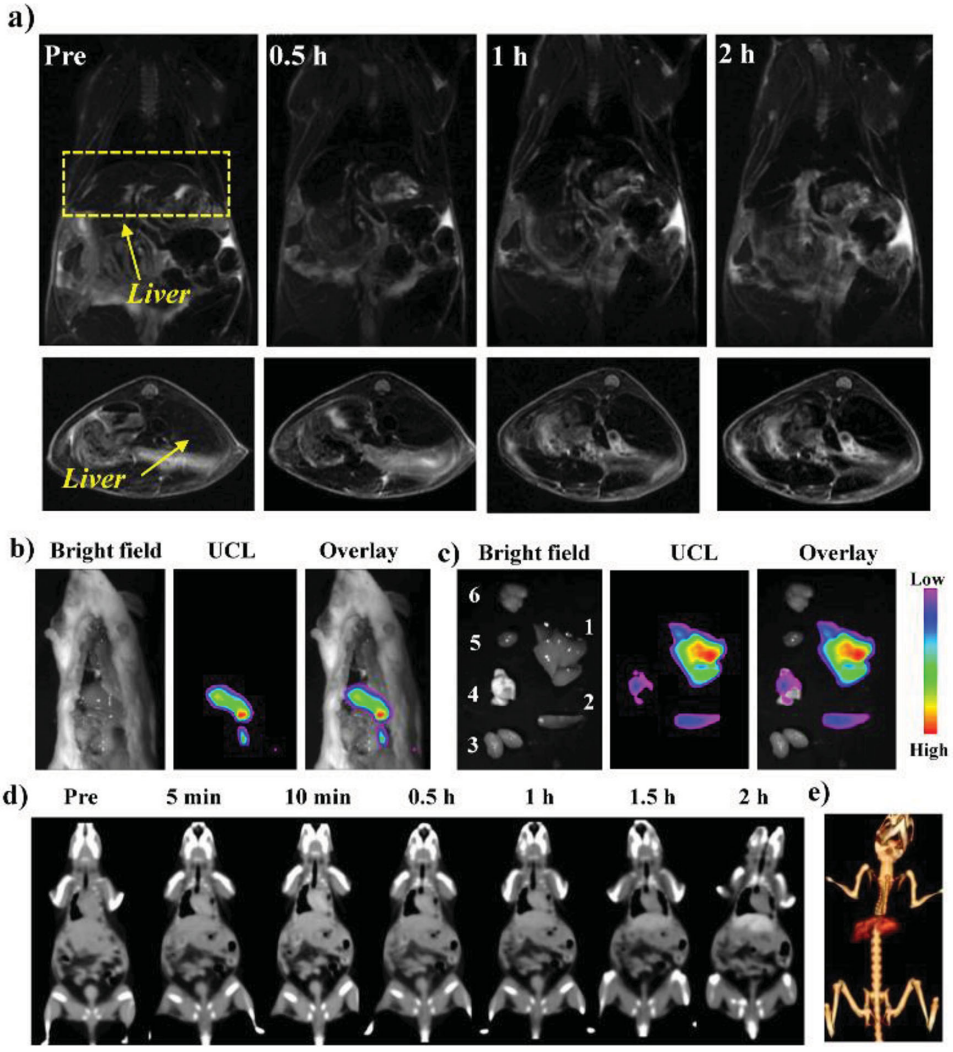

Figure 5. a) The in vivo T_2-weighted MR images of coronal (up) and transversal (down) cross-section images of the liver of mouse before and at various time points after intravenous injection of Lipo-UCNPs (30 mg Yb/kg). b,c) The UCL imaging of dissected mouse and organs after intravenous injection with Lipo-UCNPs (45 mg Yb/kg) at 2 h (1, liver; 2, spleen; 3, kidney; 4, lung; 5, heart; 6, brain.). d) In vivo CT coronal images of mice after intravenous injection of Lipo-UCNPs (240 mg/kg) at timed intervals. And the corresponding 3D rendering of in vivo CT images for e) Lipo-UCNPs at 2 h.

several main organs, including heart, liver, spleen, lung and kidney (Figure S14, Supporting Information). The mice were dissected in 1 day or 60 days after a single intravenous administration of Lipo-UCNPs (240 mg/kg) and these organs were stained with H&E. Compared to the control group, no apparent changes in cellular structure and any congestion, necrosis or hydropic degeneration are observed in organs. The results indicate that Lipo-UCNPs will cause neither acute nor chronic toxicity in vivo, reflecting that Ho^{3+}-doped UCNPs hold a great promise as multifunctional contrast agents for biomedical applications.

3. Conclusions

In conclusion, herein we have presented the first example of T_2-weighted MR imaging of Ho^{3+}-doped UCNPs, which can also be simultaneously used for UCL and CT imaging, thus enabling high performance multimodal MRI/UCL/CT imagings in single UCNPs as demonstrated by various in vitro, in vivo and ex vivo experiments. The new finding of T_2-MRI contrast enhancement by integrated sensitizer (Yb^{3+}) and activator (Ho^{3+}) in single UCNPs favors accurate MR diagnosis of brain tumors and provides a new strategy for acquiring T_2-MRI/optical imaging without fluorescent quenching. Unlike other multi-phased composite nanostructures for multimodal imaging, this Ho^{3+}-doped UCNPs are featured with simplicity of synthesis, highly efficient MRI/UCL/CT imaging without fluorescence quenching. In addition, considering that r_2 value of Ln-based NPs is roughly proportional to magnetic field strength, it is expected that Ho^{3+}-doped UCNPs will be highly attractive to act as contrast agents for ultrahigh magnetic field MRI and the relevant researches are underway.

4. Experimental Section

Chemicals: $YbCl_3{\cdot}6H_2O$, $HoCl_3{\cdot}6H_2O$, ammonium fluoride (NH_4F), 1-Octacene (90%) were obtained from Sigma-Aldrich. Oleic acid

(OA), Methanol (CH_3OH) were purchased from Shanghai Lingfeng Chemical Reagent Co., Ltd. Sodium hydroxide (NaOH) and chloroform ($CHCl_3$) were acquired from Sinopharm Chemical Reagent Co., LtD. 1, 2-Distearoyl-sn-Glycero-3-Phosphoethanolamine-N-[Amino (Polyethylene Glycol)2000] (DSPE-PEG_{2k}-NH_2) was purchased from the Avanti Polar Lipids, Inc. Lyso Tracker Green DND-26 were purchased from Invitrogen (Oregon, USA). All materials were analytical grade and used without any purification.

Synthesis of OA-$NaYbF_4$:Ho Nanoparticles: The different Ho^{3+} doped concentations of $NaYbF_4$:Ho NPs were prepared according to a thermal decomposition method. In a typical experiment of synthesizing $NaYbF_4$: 2% Ho NPs, 30 mL 1-octadecene and 15 mL oleic acid were added into the 100 mL flask followed by adding 2 mL deionized water containing $YbCl_3{\cdot}6H_2O$ (1.96 mmol), $HoCl_3{\cdot}6H_2O$ (0.04 mmol) and stired for 1 h at room temperature. Subsequently, to get rid of water, the mixture was slowly heated to 120 °C and lasted for 1 h under argon atmosphere, maintaining at 160 °C for another 1 h, and cooled down to room temperature. Later, 10 mL methanol solution of NaOH (200 mg, 5 mmol) and NH_4F (296.3 mg, 8 mmol) were added and the solution was stirred at room temperature for 3 h, following by evaporating methanol at 120 °C. After that, the solution was quickly heated to 270–280 °C and maintained for 1 h, then cooled down to room temperature. The products were washed with ethanol several times and finally dispersed in chloroform. The same above procedures were performed to synthesiz the OA-$NaYbF_4$ and OA-$NaHoF_4$.

Synthesis of Lipo-UCNPs: For good biocompatibility, the commerically available DSPE-PEG_{2k}-NH_2 was used to modify the surface of hydrophobic NPs according to previously reoported method with slight modifications.[18] Typically example: 1 mL of $NaYbF_4$: 2% Ho solution in chloroform (20 mg/mL) was added into 5 mL DSPE-PEG_{2k}-NH_2 solution in chloroform (20 mg/mL) and then stirred for 15 min. The mixture was incubated at 60 °C under vacuum in a rotary evaporator for 1 h to evaporate the solvent. Subsequently, 5 mL of water was added into the lipidic film and then sonicated for 10 min to obtain Lipo-UCNPs. In this paper, if not clearly clarified, the Lipo-UCNPs stand for $NaYbF_4$: 2%Ho with phospholipid-PEGylation.

Cell Culture and Cytotoxicity Assessment: Brain capillary endothelial cells (BCECs) were cultured at 37 °C and with 5% CO_2 in Roswell Park Memorial Institute medium (RPMI) 1640 supplemented with 15% fetal bovineserum (FBS) and 1% penicillin/streptomycin. Human glioblastoma cells U87MG were cultured at 37 °C and with 5% CO_2 in Dulbecco's Modified Eagle Medium (DMEM) supplemented with 10% fetal bovine serum (FBS) and 1% penicillin/streptomycin. The cell cytotoxicity in vitro was measured using 3-(4, 5-dimethylthiazol-2-yl)-2, 5-diphenyltetrazolium bromide (MTT) assay. Cells were seeded into a 96-well cell culture plate at 10^6/well and then incubated for one day at 37 °C under 5% CO_2. RPMI 1640/DMEM solutions of Lipo-UCNPs with different concentrations of 0, 12.5, 25, 50, 100, 200, 400 and 800 μg/mL were added to the wells. The cells were then incubated for 12 h or 24 h at 37 °C under 5% CO_2 and the cell viability was calculated by a typical MTT assy.

Cellular Confocal Fluorescence Imaging: U87MG cells were seeded at a density of 10^5 cells/well in a cell culture dish of confocol laser scaning microscopy (CLSM) and incubated for 24 h at 37 °C under 5% CO_2. The Lipo-UCNPs of cell culture media with a concentration of 800 μg/mL were added into the culture dish. After co-incubated for 2 h, the cells were washed for three times with PBS to remove the un-uptake nanoparticles. And then Lyso Tracker Green DND-26 (0.01 nM) was added into the cultured cells for additional 0.5 h, followed by nuclei staining by DAPI. Then confocal fluorescence imaging experiments were performed on an Olympus FV1000 laser-scanning microscope equipped with a CW NIR laser (λ = 980 nm). As both Lyso Tracker and UCNPs emit green light, here, the red light represcents the location of lysosomes to distinguish the fluorescence between lysosomes and UCNPs. A 100×oil immersion objective lens was used and luminescence signals were detected in the wavelength regions of 500 ~ 600 nm.

MR and CT Imaging In Vitro: The Lipo-UCNPs (0, 400, 800 μg/mL) were incubated with U87MG cells (10^6/well) at 37 °C under 5% CO_2. After co-incubation for 24 h, the cells were washed with PBS for three times, and U87MG containing Lipo-UCNPs in PBS were precipitated at the bottom of the tube after centrifugation. They were then used for MRI tests performed on a 3.0 T clinical MRI instrument (GE Signa 3.0 T). The CT tests were performed on GE discovery CT750 HD, GE Healthcare.

T_2-MR/UCL/CT Imaging In Vivo: Animal procedures were in agreement with the guidelines of the Institutional Animal Care and Use Committee. Kunming mice with average weight of 20 g were purchased from Laboratory Animal Centre, Shanghai Medical College of Fudan University, China. In vivo MR/CT/UCL imagings were conducted on a clinical MRI (GE Signa 3.0T)/CT (GE discovery CT750 HD) instrument/home-made UCL in vivo imaging system from Prof. Li's group (Advanced Materials Laboratory, Department of Chemistry, Fudan University). The mice were scanned before and after intravenous administraiton of Lipo-UCNPs at different time points. The intracranial glioblastoma-bearing mice models were established as reported.[31] Briefly, by using a stereotactic fixation device with mouse adapter, U87MG cells (5×10^5 suspended in 5 μL PBS) were implanted into the striatum (1.8 mm lateral and 3 mm of depth) of male Balb/c nude mice. And they were ready for MR imaging after inoculation for three weeks. T_2-weighted MR images of glioblastoma-bearing mice brain were collected before and 15 min, 0.5, 1, 1.5, 2 h after administration of Lipo-UCNPs with a dose of 150 μL (30 mg Yb/Kg dose) via intravenous injection. And regions of interest (ROI) with the same area were drawn on MR images before and after injection. And signal intensity of ROI in the brain tumor was then measured. T_2-weighted MR images of brain sections were acquired with the fast recovery fast spin echo (FRFSE) sequence: TR = 3000 ms, TE = 102 ms, Slice thickness = 1.5 mm, Freq. FOV = 4.5, Phase Fov = 0.8, Phase = 256, Frequency = 384.

Histological Assessment In Vivo: Kunming mice with average weight of 20 g were purchased from laboratory animal center; shanghai medical college of Fudan University. The Lipo-UCNPs at a total dose of 150 μL (240 mg/kg dose) were injected into Kunming mice via intravenous injection and mice with no injection of Lipo-UCNPs were selected as control group. Tissues were harvested from mice on 1 and 60 days post-injection or control group. Then, the tissues were H&E-stained to monitor histological changes in liver, spleen, heart, lung and kidney of mice. The histological sections were observed under an optical microscope.

Characterization: Transmission electron microscopy (TEM) images, togenther with energy-dispersive X-ray analysis (EDXA) were checked on a JEOL 200CX microscope with an accelerating voltage of 200 kV. Powder X-ray diffraction (XRD) patterns were texted on a Rigaku D/MAX-2250 V diffractometer with graphite-monochromatized CuKα radiation. Fourier transform infrared spectroscopy (FT-IR) spectra were performed on a Nicolet Avatar 370 FT-IR spectrophotometer using KBr pellets. Dynamic light scattering (DLS) measurement was conducted on Nano-Zetesizer (Malvern Instruments Ltd). The Yb, Ho concentrations of samples was measured by inductively coupled plasma optical emission spectrometry (ICP-OES). Upconversion luminescence emission spectra were collected on Fluorolog-3 Spectrofluorometer (Jobin Yvon, France) with an external 0~1W adjustable 980 nm semiconductor laser (Beijing Hi-tech Optoelectronic Co., China). CLSM images were obtained on FV 1000, Olympus, Japan.

Supporting Information

Supporting Information is available from the Wiley Online Library or from the author.

Acknowledgements

This work has been financially supported by the National Natural Science Foundation of China (Grant No. 51372260, 51132009, 21172043, 51102259), the Shanghai Rising-Star Program (Grant No. 12QH1402500), the Nano special program of the Science and Technology Commission of Shanghai (Grant No.11nm0505000), the

Development Foundation for Talents of Shanghai (Grant No.2012035). The authors thank Jianan Liu, Chen Zhang, Wenpei Fan, Jingwei Feng, Linlin Zhang, Heliang Yao from Shanghai Institute of Ceramics, Chinese Academy of Sciences for useful discussions. The authors thank Jie Fan from Huashang Hospital, Fudan University for histological analysis.

Received: May 19, 2014
Revised: July 14, 2014
Published online: August 22, 2014

[1] a) R. Weissleder, M. J. Pittet, *Nature* **2008**, *452*, 580; b) M. Bottrill, L. Kwok, N. J. Long, *Chem. Soc. Rev.* **2006**, *35*, 557; c) R. J. Gillies, N. Raghunand, G. S. Karczmar, Z. M. Bhujwalla, *J. Magn. Reson. Imaging* **2002**, *16*, 430; d) A. P. Pathak, B. Gimi, K. Glunde, E. Ackerstaff, D. Artemov, Z. M. Bhujwalla, *Method. Enzymol.* **2004**, *386*, 3; e) R. P. Mason, D. Zhao, J. Pacheco-Torres, W. Cui, V. D. Kodibagkar, P. K. Gulaka, G. Hao, P. Thorpe, E. W. Hahn, P. Peschke, *Q. J. Nucl. Med. Mol. Imaging* **2010**, *54*, 259.

[2] a) P. Caravan, J. J. Ellison, T. J. McMurry, R. B. Lauffer, *Chem. Rev.* **1999**, *99*, 2293; b) Y. W. Jun, J. H. Lee, J. Cheon, *Angew. Chem. Int. Ed.* **2008**, *47*, 5122.

[3] a) J. Park, K. An, Y. Hwang, J. G. Park, H. J. Noh, J. Y. Kim, J. H. Park, N. M. Hwang, T. Hyeon, *Nat. Mater.* **2004**, *3*, 891; b) J. H. Lee, Y. M. Huh, Y. W. Jun, J. W. Seo, J. T. Jang, H. T. Song, S. Kim, E. J. Cho, H. G. Yoon, J. S. Suh, J. Cheon, *Nat. Med.* **2007**, *13*, 95; c) W. S. Seo, J. H. Lee, X. Sun, Y. Suzuki, D. Mann, Z. Liu, M. Terashima, P. C. Yang, M. V. McConnell, D. G. Nishimura, H. Dai, *Nat. Mater.* **2006**, *5*, 971; d) Z. Zhou, D. Huang, J. Bao, Q. Chen, G. Liu, Z. Chen, X. Chen, J. Gao, *Adv. Mater.* **2012**, *24*, 6223.

[4] a) H. B. Na, I. C. Song, T. Hyeon, *Adv. Mater.* **2009**, *21*, 2133; b) J. W. M. Bulte, D. L. Kraitchman, *NMR Biomed.* **2004**, *17*, 484.

[5] a) A. Louie, *Chem. Rev.* **2010**, *110*, 3146; b) D. E. Lee, H. Koo, I. C. Sun, J. H. Ryu, K. Kim, I. C. Kwon, *Chem. Soc. Rev.* **2012**, *41*, 2656.

[6] a) A. Quarta, R. Di Corato, L. Manna, S. Argentiere, R. Cingolani, G. Barbarella, T. Pellegrino, *J. Am. Chem. Soc.* **2008**, *130*, 10545; b) I. P. Chang, K. C. Hwang, C. S. Chiang, *J. Am. Chem. Soc.* **2008**, *130*, 15476; c) P. Howes, M. Green, A. Bowers, D. Parker, G. Varma, M. Kallumadil, M. Hughes, A. Warley, A. Brain, R. Botnar, *J. Am. Chem. Soc.* **2010**, *132*, 9833.

[7] a) C. Y. Ang, L. Giam, Z. M. Chan, A. W. H. Lin, H. Gu, E. Devlin, G. C. Papaefthymiou, S. T. Selvan, J. Y. Ying, *Adv. Mater.* **2009**, *21*, 869; b) D. K. Yi, S. T. Selvan, S. S. Lee, G. C. Papaefthymiou, D. Kundaliya, J. Y. Ying, *J. Am. Chem. Soc.* **2005**, *127*, 4990; c) Z. Wang, L. Wu, M. Chen, S. Zhou, *J. Am. Chem. Soc.* **2009**, *131*, 11276.

[8] a) S. Gai, C. Li, P. Yang, J. Lin, *Chem. Rev.* **2014**, *114*, 2343; b) C. Liu, Y. Hou, M. Gao, *Adv. Mater.* **2014**, DOI: 10.1002/adma.201305535; c) H. H. Gorris, O. S. Wolfbeis, *Angew. Chem. Int. Ed.* **2013**, *52*, 3584; d) Z. Gu, L. Yan, G. Tian, S. Li, Z. Chai, Y. Zhao, *Adv. Mater.* **2013**, *25*, 3758; e) A. Gnach, A. Bednarkiewicz, *Nano Today* **2012**, *7*, 532; f) Y. Liu, D. Tu, H. Zhu, X. Chen, *Chem. Soc. Rev.* **2013**, *42*, 6924; g) G. Chen, H. Qiu, P. N. Prasad, X. Chen, *Chem. Rev.* **2014**, *114*, 5161.

[9] a) L. Cheng, K. Yang, Y. Li, J. Chen, C. Wang, M. Shao, S. T. Lee, Z. Liu, *Angew. Chem. Int. Ed.* **2011**, *50*, 7385; b) S. L. Gai, P. P. Yang, C. X. Li, W. X. Wang, Y. L. Dai, N. Niu, J. Lin, *Adv. Funct. Mater.* **2010**, *20*, 1166; c) A. Xia, Y. Gao, J. Zhou, C. Li, T. Yang, D. Wu, L. Wu, F. Li, *Biomaterials* **2011**, *32*, 7200; d) X. Zhu, J. Zhou, M. Chen, M. Shi, W. Feng, F. Li, *Biomaterials* **2012**, *33*, 4618; e) L. Zhang, Y. S. Wang, Y. Yang, F. Zhang, W. F. Dong, S. Y. Zhou, W. H. Pei, H. D. Chen, H. B. Sun, *Chem. Commun.* **2012**, *48*, 11238.

[10] T. R. Sathe, A. Agrawal, S. Nie, *Anal. Chem.* **2006**, *78*, 5627.

[11] a) I. Bertini, F. Capozzi, C. Luchinat, G. Nicastro, Z. C. Xia, *J. Phys. Chem.* **1993**, *97*, 6351; b) K. Kattel, J. Y. Park, W. Xu, H. G. Kim, E. J. Lee, B. A. Bony, W. C. Heo, J. J. Lee, S. Jin, J. S. Baeck, Y. Chang, T. J. Kim, J. E. Bae, K. S. Chae, G. H. Lee, *ACS Appl. Mater. Interfaces* **2011**, *3*, 3325.

[12] L. Vander Elst, A. Roch, P. Gillis, S. Laurent, F. Botteman, J. W. Bulte, R. N. Muller, *Magn. Reson. Med.* **2002**, *47*, 1121.

[13] a) S. Viswanathan, Z. Kovacs, K. N. Green, S. J. Ratnakar, A. D. Sherry, *Chem. Rev.* **2010**, *110*, 2960; b) M. Norek, J. A. Peters, *Prog. Nucl. Magn. Reson. Spectrosc.* **2011**, *59*, 64.

[14] a) H. Xing, W. Bu, Q. Ren, X. Zheng, M. Li, S. Zhang, H. Qu, Z. Wang, Y. Hua, K. Zhao, L. Zhou, W. Peng, J. Shi, *Biomaterials* **2012**, *33*, 5384; b) Y. Liu, K. Ai, J. Liu, Q. Yuan, Y. He, L. Lu, *Angew. Chem. Int. Ed.* **2012**, *51*, 1437.

[15] a) H. Y. Xing, W. B. Bu, S. J. Zhang, X. P. Zheng, M. Li, F. Chen, Q. J. He, L. P. Zhou, W. J. Peng, Y. Q. Hua, J. L. Shi, *Biomaterials* **2012**, *33*, 1079; b) Q. Xiao, W. Bu, Q. Ren, S. Zhang, H. Xing, F. Chen, M. Li, X. Zheng, Y. Hua, L. Zhou, W. Peng, H. Qu, Z. Wang, K. Zhao, J. Shi, *Biomaterials* **2012**, *33*, 7530; c) F. Chen, S. J. Zhang, W. B. Bu, X. H. Liu, Y. Chen, Q. J. He, M. Zhu, L. X. Zhang, L. P. Zhou, W. J. Peng, J. L. Shi, *Chem. Eur. J.* **2010**, *19*, 11254.

[16] a) J. T. Huse, E. C. Holland, *Nat. Rev. Cancer* **2010**, *10*, 319; b) J. Y. Zhou, E. Tryggestad, Z. B. Wen, B. Lal, T. T. Zhou, R. Grossman, S. L. Wang, K. Yan, D. X. Fu, E. Ford, B. Tyler, J. Blakeley, J. Laterra, P. C. M. van Zijl, *Nat. Med.* **2011**, *17*, 130.

[17] a) D. Ni, J. Zhang, W. Bu, H. Xing, F. Han, Q. Xiao, Z. Yao, F. Chen, Q. He, J. Liu, S. Zhang, W. Fan, L. Zhou, W. Peng, J. Shi, *ACS Nano* **2014**, *8*, 1231; b) Q. Xiao, X. Zheng, W. Bu, W. Ge, S. Zhang, F. Chen, H. Xing, Q. Ren, W. Fan, K. Zhao, Y. Hua, J. Shi, *J. Am. Chem. Soc.* **2013**, *135*, 13041; c) J. Liu, W. Bu, L. Pan, J. Shi, *Angew. Chem. Int. Ed.* **2013**, *52*, 4375.

[18] L. L. Li, R. Zhang, L. Yin, K. Zheng, W. Qin, P. R. Selvin, Y. Lu, *Angew. Chem. Int. Ed.* **2012**, *51*, 6121.

[19] D. Liu, W. Wu, J. Ling, S. Wen, N. Gu, X. Zhang, *Adv. Funct. Mater.* **2011**, *21*, 1498.

[20] R. Kumar, M. Nyk, T. Y. Ohulchanskyy, C. A. Flask, P. N. Prasad, *Adv. Funct. Mater.* **2009**, *19*, 853–859.

[21] a) F. Chen, W. Bu, S. Zhang, J. Liu, W. Fan, L. Zhou, W. Peng, J. Shi, *Adv. Funct. Mater.* **2013**, *23*, 298; b) H. Guo, Z. Li, H. Qian, Y. Hu, I. N. Muhammad, *Nanotechnology* **2010**, *21*, 125602; c) Y. I. Park, J. H. Kim, K. T. Lee, K.-S. Jeon, H. B. Na, J. H. Yu, H. M. Kim, N. Lee, S. H. Choi, S.-I. Baik, H. Kim, S. P. Park, B.-J. Park, Y. W. Kim, S. H. Lee, S.-Y. Yoon, I. C. Song, W. K. Moon, Y. D. Suh, T. Hyeon, *Adv. Mater.* **2009**, *21*, 4467; d) J. Zhou, M. Yu, Y. Sun, X. Zhang, X. Zhu, Z. Wu, D. Wu, F. Li, *Biomaterials* **2011**, *32*, 1148.

[22] K. M. Donahue, D. Burstein, W. J. Manning, M. L. Gray, *Magnet. Reson. Med.* **1994**, *32*, 66.

[23] a) J. Qin, S. Laurent, Y. S. Jo, A. Roch, M. Mikhaylova, Z. M. Bhujwalla, R. N. Muller, M. Muhammed, *Adv. Mater.* **2007**, *19*, 1874; b) G. K. Das, N. J. J. Johnson, J. Cramen, B. Blasiak, P. Latta, B. Tomanek, F. C. J. M. van Veggel, *J. Phys. Chem. Lett.* **2012**, *3*, 524.

[24] a) M. Rohrer, H. Bauer, J. Mintorovitch, M. Requardt, H.-J. Weinmann, *Invest. Radiol.* **2005**, *40*, 715; b) Y. X. Wang, *Quant. Imaging. Med. Surg.* **2011**, *1*, 35.

[25] M. Norek, G. A. Pereira, C. F. G. C. Geraldes, A. Denkova, W. Zhou, J. A. Peters, *J. Phys. Chem. C* **2007**, *111*, 10240.

[26] J. T. Rosenberg, J. M. Kogot, D. D. Lovingood, G. F. Strouse, S. C. Grant, *Magn. Reson. Med.* **2010**, *64*, 871.

[27] G. Le Duc, I. Miladi, C. Alric, P. Mowat, E. Brauer-Krisch, A. Bouchet, E. Khalil, C. Billotey, M. Janier, F. Lux, T. Epicier, P. Perriat, S. Roux, O. Tillement, *ACS Nano* **2011**, *5*, 9566.

[28] a) O. Ehlert, R. Thomann, M. Darbandi, T. Nann, *ACS Nano* **2008**, *2*, 120–124; b) Q. Zhan, J. Qian, H. Liang, G. Somesfalean, D. Wang, S. He, Z. Zhang, S. Andersson-Engels, *ACS Nano* **2011**, *5*, 3744.

[29] F. Wang, X. Liu, *J. Am. Chem. Soc.* **2008**, *130*, 5642.

[30] D. Kim, S. Park, J. H. Lee, Y. Y. Jeong, S. Jon, *J. Am. Chem. Soc.* **2007**, *129*, 7661.

[31] H. Yan, L. Wang, J. Wang, X. Weng, H. Lei, X. Wang, L. Jiang, J. Zhu, W. Lu, X. Wei, C. Li, *ACS Nano* **2012**, *6*, 410.